



Approximated and Iterative Power Flow Algorithms for Islanded DC Microgrids

Elson N.M. Silva, Anselmo B. Rodrigues, Maria da Guia da Silva*

Electrical Engineering Department, UFMA, São Luís-MA, 65080-805, Brazil

ARTICLE INFO

Keywords:

Admittance Summation Method
Current Summation Method
Islanded DC Microgrid
Modified Augmented Nodal Analysis
Probabilistic Power Flow

ABSTRACT

The main approach used to model uncertainties in microgrid planning is the Probabilistic Power Flow (PPF). However, this technique has a high computational cost due to the need to solve a system of nonlinear equations for different scenarios of microgrid operation. This paper aims to propose low-cost computational power flow algorithms to evaluate nodal voltages in islanded Direct Current (DC) microgrids under uncertainty. An approximated power flow is proposed based on the Admittance Summation Method for radial microgrids. In addition, iterative power flow algorithms, previously developed by the authors for Alternating Current (AC) microgrids, have been adapted for DC microgrids. The proposed iterative and approximated algorithms were combined with Monte Carlo Simulation to obtain a PPF method. The proposed methods were tested and validated in relation to the Newton-Raphson Method in DC radial microgrids with 33 and 906 nodes and in DC meshed microgrids with 33 e 144 nodes. The results showed that the developed methods have good accuracy and obtain considerable saving in the computational cost of the PPF.

1. Introduction

A microgrid can be described as a cluster of loads and generators that can operate in an interconnected or islanded way from the electrical distribution network [1, 2]. The islanded operation occurs when there is a disturbance in the utility's system and the microgrid is automatically disconnected from the Common Coupling Point (CCP). During the islanded operation, the microgrid loads are supplied by their own native generation. Therefore, it is expected that the reliability of the microgrid will be improved.

An important aspect that has gained importance in the design of microgrids is the application of Direct Current (DC) microgrids and hybrid microgrids (DC and Alternating Current (AC)) [3, 4]. The use of DC voltage is motivated by the following facts: (i) increased DC loads (Light-Emitting Diode (LED) lamps, computers, printers, etc.); (ii) DC renewable Distributed Generation (DG) (solar photovoltaic and fuel cells); (iii) insertion of battery energy storage systems to increase the use of renewable DG. The DC microgrids can offer the following advantages when compared with AC microgrids [5],[6]: (i) minimization of conversion losses; (ii) greater power transfer capacity; (iii) elimination of the need for frequency synchronism. At this point, it is important to mention that the algorithms proposed in this paper are oriented towards

DC microgrids, that is, hybrid AC-DC microgrids are not considered.

The planning of the microgrid must ensure that the islanded operation satisfies the power quality constraints related to the voltage and frequency. However, the presence of uncertainties in the microgrid parameters (i.e., output power of the renewable DG, load fluctuations and equipment outages) gives rise to a risk of violation of these constraints. The main tool used to model uncertainties in microgrid planning is the Probabilistic Power Flow (PPF) [7]. The most used technique in the PPF solution is the Monte Carlo Simulation (MCS) [7]. The main disadvantage of MCS is its high computational cost due to the need to solve the power flow equations for several randomly selected system scenarios. Therefore, an important prerequisite that must be considered in the design of the power flow algorithms for the planning of microgrids under uncertainty is the computational cost.

The main characteristic that differentiates the power flow algorithms for islanded microgrids from the conventional power flow is the absence of a single slack node with infinity capacity to supply the loads plus the loss. Because of this, the power flow of the microgrid called Power Flow with Multiple Slack Nodes (FMS).

The FMS algorithms for DC microgrids can be classified as follows [8]-[14]:

* Corresponding author.

E-mail address: guia.maria@ufma.br (M. da Guia da Silva).

<https://doi.org/10.1016/j.epsr.2022.108972>

Received 3 April 2021; Received in revised form 7 November 2022; Accepted 12 November 2022

Available online 22 November 2022

0378-7796/© 2022 Elsevier B.V. All rights reserved.

- i) Jacobian based methods: apply the Newton-Raphson Method (NRM) and its variants with the Jacobian matrix calculation to solve the nonlinear system associated with the power flow equations [8],[9],[10].
- ii) Backward/Forward Sweep Methods: explore the radial topology to iteratively solve the power flow equations based on the Fixed-Point Method (FPM) and Kirchhoff's laws [11].
- iii) Gauss-Zbus Method (GZM): combine the nodal analysis of the matrix with the FPM to obtain the power solution through an iterative process [12].
- iv) Approximations: use the first order Taylor expansion to linearize the current injection of the nodal matrix analysis [13, 14].

The approximated algorithms do not obtain the exact solution of the power flow equations. However, they have great potential to reduce the computational cost of PPF. This advantage is due to the fact that the approximate algorithms do not require the iterative solution of the power flow equations. This potential can be explored more intensely through the backward/forward sweep methods, as these methods are free from the solution of linear systems. Despite this, no approximate power flow based on backward/forward sweep methods has been developed for radial microgrids. Thus, it is interesting to develop approximate power flow algorithms with good accuracy and low computational cost for DC microgrids with radial topology. The development of these algorithms is very important for several application scenarios that demand the solution of many FMS for DC microgrids (FMS-DC), for example: (i) sensitivity analysis; (ii) propagation of uncertainties; (ii) estimation of power quality and reliability indices; (iii) security assessment; (iv) optimization of microgrids based on meta-heuristic algorithms (reconfiguration, DG dispatch, DG placement, etc.).

This paper aims to propose new FMS algorithms for DC microgrids with radial and meshed topologies. These algorithms are derived based on the following techniques: Admittance Summation Method (ASM) [15] and Current Summation Method (CSM) [16] for radial microgrids and Modified Augmented Nodal Analysis (MANA) [17] and GZM [18] for meshed microgrids. Linear models for loads and generators are derived through linear regression and Taylor's expansion. These models are used by ASM to calculate the nodal voltages in radial microgrids without the need for an iterative process. Additionally, CSM, GZM and MANA are combined with the principle of superposition and the solution of a quadratic equation to obtain FMS-DC based on iterative FMS for AC microgrids previously developed by the authors [19]. In all, three versions of FMS-DC are proposed in the paper: one approximate and two iteratives. These versions of the FMS-DC are incorporated into the MCS to generate a PPF to estimate probabilistic indices for islanded DC microgrids. The proposed FMS-DC algorithms were tested and validated in radial microgrids with 33 [20] and 906 [21] nodes and in meshed microgrids with 33 [20] and 144 [21] nodes. The results showed that the developed methods have good accuracy to estimate state variables and probabilistic indices in islanded DC microgrids and considerably reduce the computational cost of PPF.

Thus, the main contributions of this paper are:

- Introduction of a non-iterative ASM-based algorithm to solve the FMS in radial DC microgrids.
- Proposition of an iterative method based on GZM and MANA for the FMS solution in meshed DC microgrids.
- Proposition of an iterative technique based on CSM for the calculation of FMS in radial DC microgrids.

The rest of this paper is organized as follows. In section 2, an analysis of publications correlated with the methods proposed in this paper is presented. Section 3 presents the non-iterative approach designed to solve the FMS in radial DC microgrids. The iterative algorithms based on CSM and GZM for FMS on radial and meshed DC microgrids, respectively, are explained in section 4. Section 5 describes the uncertainty

modelling used in PPF for DC microgrids. The tests results with the proposed algorithms for the FMS-DC are presented in section 6. Finally, the main conclusions and findings are summarized in section 7.

2. Related Work

References [11, 12] introduced FPM variants based on backward/forward sweep techniques and GZM to solve the FMS-DC. The attraction for the developments of these variants is their low computational cost compared to the NRM, as they do not require the assembly and solution of the Jacobian system for each iteration. Like [11] and [12], the iterative methods proposed in this paper have the FPM as common ancestor to achieve a low computational cost algorithms to solve the FMS-DC. However, the development of the iteration function of the methods proposed in this paper is based on power flow algorithms, previously developed by the authors, for islanded AC microgrids [19]. In fact, the authors simplified the solution of the nonlinear sub-problem in the AC iteration function to obtain new algorithms for DC microgrids.

The authors of [13] and [14] proposed linear approximations to solve the FMS-DC based on nodal analysis and Taylor series. These approximations require the solution of a linear system to evaluate the nodal voltages. Thus, the computational cost of the algorithms proposed in [13] and [14] can be high in applications that demand the solution of several FMS-DC, for example, the PPF. In this paper, the authors introduced approximated methods to solve the FMS-DC based on the backward-forward sweep technique and ASM. The main advantage of the sweep technique is that it is matrix free and, consequently, has a low computational in relation to the nodal analysis approximations. Therefore, the sweep techniques proposed in this paper are more suitable for PPF. Furthermore, the approximate method proposed in this paper has better accuracy when linearization is performed using linear regression instead of Taylor series. Finally, it is important to mention that there is no record in the technical literature about the approximate method designed for AC or DC islanded microgrids based on backward/forward sweep. In this way, this paper adds a significant advance in the state of the art related to approximate power flow algorithms for microgrids.

3. Equivalent Circuits and Non-Iterative Admittance Summation Method

The derivation of the approximated FMS-DC for radial microgrids is based on the equivalent linear circuits for loads and generators. These circuits are developed based on two techniques: first order Taylor expansion [22] and linear regression [23]. The equivalent circuit of the loads is obtained by Taylor expansion from his currents extractions as follows [22]:

$$I_{d_k} = \frac{P_{d_k}}{V_k} \approx P_{d_k}(2 - V_k) = 2P_{d_k} - P_{d_k}V_k \quad (1)$$

Where: I_{d_k} , P_{d_k} and V_k are the current extraction, the active power and the voltage magnitude for the load connected to node k .

On the other hand, the linearization of I_k by means of linear regression results in (2).

$$I_k = \frac{P_{d_k}}{V_k} \approx P_{d_k}(\hat{a}V_k + \hat{b}) = \hat{a}P_{d_k}V_k + P_{d_k}\hat{b} \quad (2)$$

Where: \hat{a} and \hat{b} are the coefficients of the linear regression model to approximate V_k^{-1} .

From (1) and (2), it is possible to obtain the equivalent circuit shown in Fig. 1(A). The parameters of this circuit are defined as follows:

- i) Taylor expansion: $I_{d_k}^{eq} = 2P_{d_k}$ and $G_{d_k}^{eq} = -P_{d_k}$;
- ii) Linear Regression: $I_{d_k}^{eq} = P_{d_k}\hat{b}$ and $G_{d_k}^{eq} = \hat{a}P_{d_k}$.

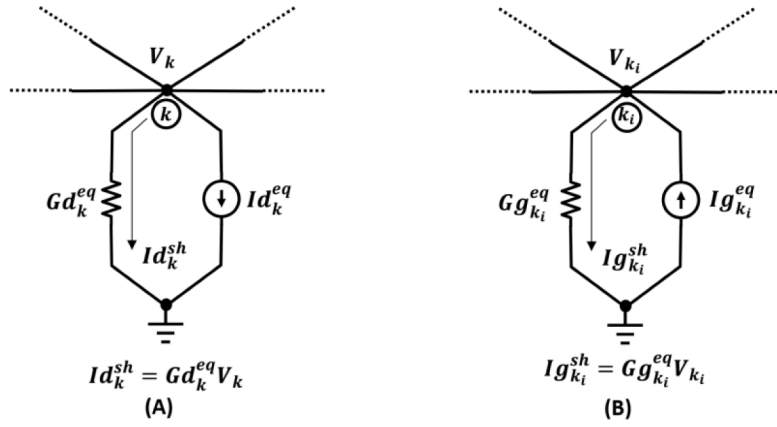


Fig. 1. (A) Linearized equivalent circuit for loads. (B) Linearized equivalent circuit for generators.

Using the same approach applied to loads, the linearization of current injections for a DG with power-based droop control is given by:

i) Taylor expansion:

$$I_{g_i}^P = \frac{Pg_i^P(V_{k_i})}{V_{k_i}} \approx \left[2 \left(Pg_i^{r,P} + \frac{V_i^{r,P}}{Kg_i^P} \right) - \frac{1}{Kg_i^P} \right] - \left(Pg_i^{r,P} + \frac{V_i^{r,P}}{Kg_i^P} \right) V_{k_i} \quad (3)$$

ii) Linear Regression:

$$I_{g_i}^P = \frac{Pg_i^P(V_{k_i})}{V_{k_i}} \approx \left(Pg_i^{r,P} + \frac{V_i^{r,P}}{Kg_i^P} \right) \hat{a} V_{k_i} + \left[\left(Pg_i^{r,P} + \frac{V_i^{r,P}}{Kg_i^P} \right) \hat{b} - \frac{1}{Kg_i^P} \right] \quad (4)$$

Where:

$$Pg_i^P(V_{k_i}) = Pg_i^{r,P} + \frac{1}{Kg_i^P} (V_i^{r,P} - V_{k_i}) \quad (5)$$

$I_{g_i}^P$ and $Pg_i^P(V_{k_i})$ are current injection and active output power for DG i with power-based droop control [8], respectively.

$Pg_i^{r,P}$ and $V_i^{r,P}$ are the reference values for the active output power and the voltage magnitude of the DG i with power-based droop control, respectively.

Kg_i^P is the constant for the power-based droop control in DG i .

k_i is the node to which DG i is connected.

From (3) and (4), it is possible to obtain the equivalent circuit shown in Fig. 1(B). The parameters of this circuit are defined as follows:

i) Taylor expansion: $I_{g_{k_i}}^{eq} = 2 \left(Pg_i^{r,P} + \frac{V_i^{r,P}}{Kg_i^P} \right) - \frac{1}{Kg_i^P}$ and $Gg_{k_i}^{eq} = \left(Pg_i^{r,P} + \frac{V_i^{r,P}}{Kg_i^P} \right)$;

ii) Linear Regression: $I_{g_{k_i}}^{eq} = \left(Pg_i^{r,P} + \frac{V_i^{r,P}}{Kg_i^P} \right) \hat{b} - \frac{1}{Kg_i^P}$ and $Gg_{k_i}^{eq} = - \left(Pg_i^{r,P} + \frac{V_i^{r,P}}{Kg_i^P} \right) \hat{a}$.

If a DG has current based droop control, then it is not necessary to apply Taylor expansion or linear regression to obtain a linear circuit, as the current injection for this type of generator is already linear according to (6) [10],[11],[13].

$$I_{g_i}^I(V_{k_i}) = I_{g_i}^{r,I} + \frac{1}{Kg_i^I} (V_i^{r,I} - V_{k_i}) \quad (6)$$

Where:

$I_{g_i}^I(V_{k_i})$ is the current injection for a DG with current based droop control.

$I_{g_i}^{r,I}$ and $V_i^{r,I}$ are the current and voltage references values, respectively, for current based droop control in DG i

Kg_i^I is the constant for the current based droop control in DG i .

DC microgrids also have renewable DG that are not dispatchable due to the intermittence in their power outputs [13]. In this way, renewable DG are modelled as constant power sources. Consequently, the equivalent circuit for renewable DG is similar to that developed for loads.

If the loads and DG of a utility connected to DC microgrid can be represented by equivalent linear circuits, then the nodal voltages can be determined in a non-iterative way using the ASM [15]. Basically, the backward sweep of the ASM reduces the linear equivalent circuit associated with the distribution network based on the Norton's equivalent circuit. The process of reducing the circuit performed in the ASM is illustrated in Fig 2(A). The equivalent currents sources and equivalent shunt conductances obtained in the backward sweep of the ASM are defined according to (7)-(11) [15].

i) Initialization:

$$I_k^{EDS} = 0; G_k^{EDS} = 0 \quad \forall k = 1, \dots, N^{node} \quad (7)$$

$$I_{k_i}^{EDS} = I_{k_i}^{EDS} - I_{g_{k_i}}^{eq}; G_{k_i}^{EDS} = G_{k_i}^{EDS} + G_{g_{k_i}}^{eq} \quad \forall i \in \mathcal{G} \quad (8)$$

$$I_k^{EDS} = I_k^{EDS} + I_{d_k}^{eq}; G_k^{EDS} = G_k^{EDS} + G_{d_k}^{eq} \quad \forall k \in \mathcal{D} \quad (9)$$

ii) Backward Sweep:

$$I_{k_j}^{EDS} = I_{k_j}^{EDS} + D_j^{bran} I_{m_j}^{EDS} \quad \forall i = N^{bran}, \dots, 1; j \leftarrow \mathcal{B}_i^{sort} \quad (10)$$

$$G_{k_j}^{EDS} = G_{k_j}^{EDS} + D_j^{bran} G_{m_j}^{EDS} \quad \forall i = N^{bran}, \dots, 1; j \leftarrow \mathcal{B}_i^{sort} \quad (11)$$

\mathcal{G} and \mathcal{D} are sets of generation and demand nodes of the microgrid. N^{bran} and N^{node} are the numbers of branches and nodes in the microgrid.

\mathcal{B}_i^{sort} is a list of branches in which the elements are sorted in ascending order by layer. The branch's layer is the number of branches between its receiving node and the root node.

k_j and m_j are the sending and receiving nodes associated with branch j , respectively.

r_j^{bran} is the series resistance for branch j .

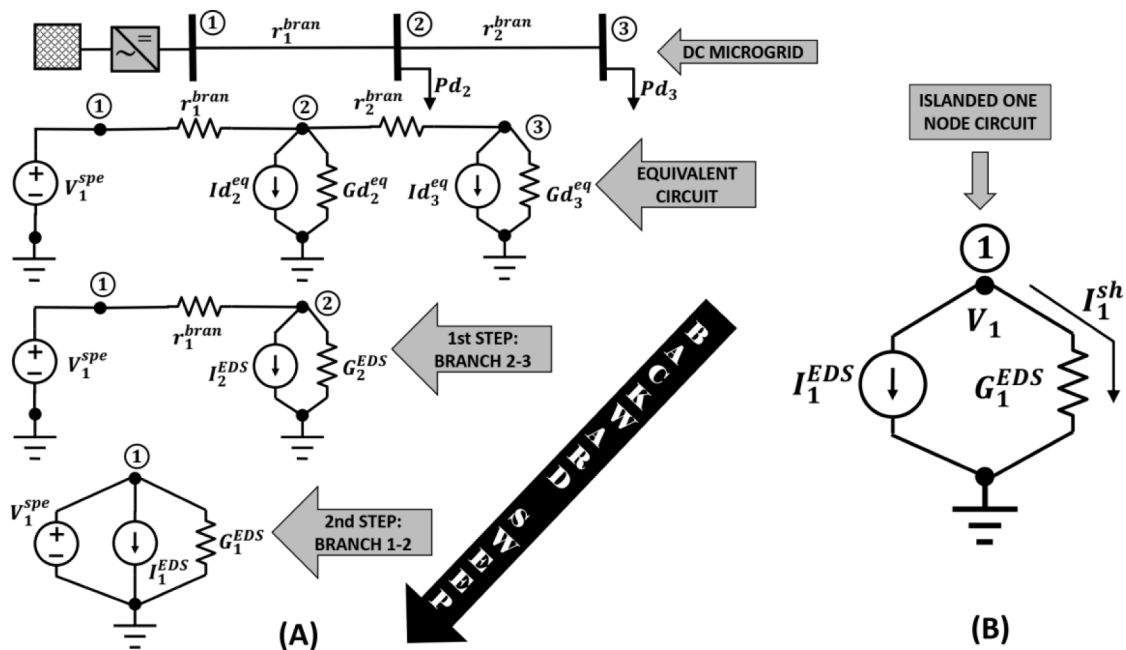


Fig. 2. (A) Circuit reduction in the backward sweep. (B) Islanded one node circuit.

$I_{k_j}^{EDS}$ and $G_{k_j}^{EDS}$ are the equivalent current and the equivalent conductance downstream of the k_j node, respectively.

$D_j^{bran} = (1 + r_j^{bran} G_{m_j}^{EDS})^{-1}$ is a dimensionless factor related to branch j [15].

Next, the nodal voltages are evaluated considering each equivalent circuit from the source to the loads (forward sweep) and applying equations (12)-(13) [15].

$$V_1 = V_1^{spe} \quad (12)$$

$$V_{m_j} = D_j^{bran} (V_{k_j} - r_j^{bran} I_{m_j}^{EDS}) \quad \forall i = 1, \dots, N^{bran}; j \leftarrow \mathcal{D}_i^{sort} \quad (13)$$

Where V_1^{spe} is the specified value of the voltage magnitude at node #1 which is selected as the root node (CCP).

In DC microgrids connected to the utility system, the voltage at the root node is specified (equation (12)). Consequently, it is possible to determine the nodal voltages remaining in the forward sweep (equation (13)), since the number of branches N^{bran} in a radial network is equal to $N^{node} - 1$. On the contrary, in islanded microgrids the voltage of CCP, V_1 is unknown. Therefore, the forward sweep is underdetermined, since there are more variables (N^{node}) than equations in the forward sweep ($N^{bran} = N^{node} - 1$) to determine the state of the microgrid in the islanded mode. This problem can be overcome by remembering that the reduction of the equivalent circuit of the distribution network is carried out until that circuit of a node composed only by the root/source node is obtained. This equivalent circuit is shown at the bottom of the Fig. 2(A). In utility connected operation there is a voltage source, representing the utility supply point, in parallel with Norton's final equivalent circuit. However, in the islanded operation there is only the final Norton equivalent circuit, as shown in Fig. 2(B). This circuit can be used to eliminate the underdetermined characteristic of the forward sweep by applying the Kirchhoff's Current Law to node 1 of Fig. 2(B). In this way, the voltage V_1 is calculated as follows:

$$I_1^{EDS} + I_1^{sh} = 0 \Rightarrow I_1^{EDS} + G_1^{EDS} V_1 = 0 \Rightarrow V_1 = -I_1^{EDS} / G_1^{EDS} \quad (14)$$

Once the voltage V_1 is determined using (14), it is possible to expand the non-iterative ASM to evaluate the voltages in islanded radial DC

microgrids. Therefore, the voltages for the utility connected and islanded microgrids can be evaluated using the flowchart shown in Fig. 3, where:

flag is true (false) if the microgrid is connected to the utility (islanded).

The input data for the approximated FMS-DC for radial microgrids are: *flag*, V_1^{spe} , \mathcal{D}^{sort} and data for branches, loads and DG.

4. Iterative FMS-DC Algorithms for Radial and Meshed Microgrids

The iterative FMS algorithms for radial and meshed AC microgrids proposed in [19] are based on the derivation of a linear circuit associated with an iteration of the CSM [16] and GZM [18] with MANA [17], respectively. These linear circuits are obtained by replacing loads and generators with current sources and the CCP with a voltage source. The linear circuit allows nodal voltages to be expressed as functions of the CCP voltage based on the superposition principle. The superposition principle is applied by type of source (current and voltage). The expression of the voltages as a function of the CCP voltage allows this voltage to be evaluated by solving a small nonlinear subproblem via NRM. This subproblem has three unknowns: angular frequency and magnitude and angle of the voltage in the CCP.

After calculating the CCP voltage, the remaining nodal voltages are obtained by adding the nodal voltage components associated with the voltage and current sources.

The iterative technique summarized above can be applied directly to radial and meshed DC microgrids. The main difference between the iterative FMS for AC and DC islanded microgrids is that the angular frequency and voltage angles do not exist in DC microgrids. Consequently, there is only one unknown in the subproblem: the voltage magnitude in the CCP (V_1). Therefore, it is necessary to use only one equation to determine the CCP voltage: the active power balance equation defined in (15).

$$P_{g_{tot}}^P + P_{g_{tot}}^I + P_{g_{tot}}^R = P_{d_{tot}} + P_{tot}^{loss} \quad (15)$$

Where:

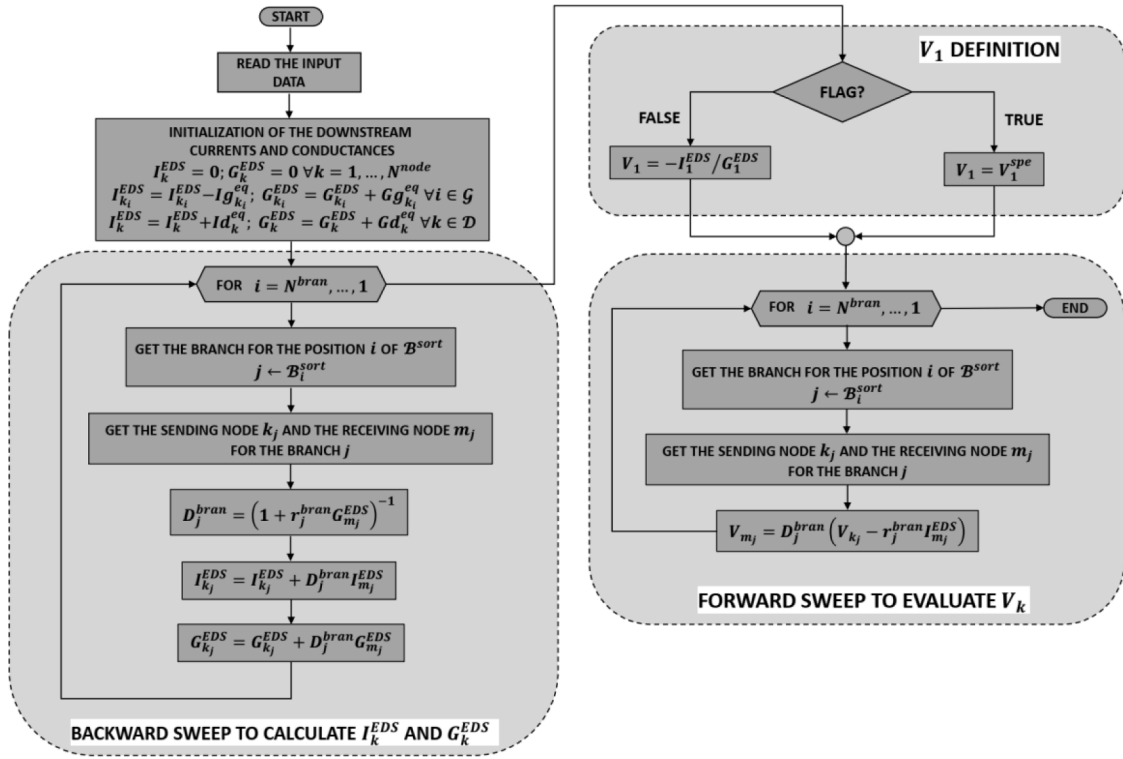


Fig. 3. Flowchart for the approximated FMS for radial DC microgrids.

$$Pg_{tot}^P = \sum_{i \in \mathcal{G}^P} Pg_i^P(V_{k_i}) = \sum_{i \in \mathcal{G}^P} \left[Pg_i^{r,P} + \frac{1}{Kg_i^P} (V_i^{r,P} - V_{k_i}) \right] \quad (16)$$

$$Pg_{tot}^I = \sum_{i \in \mathcal{G}^I} Pg_i^I(V_{k_i}) = \sum_{i \in \mathcal{G}^I} [V_{k_i} \times Ig_i^I(V_{k_i})] = \sum_{i \in \mathcal{G}^I} \left[V_{k_i} \left(Ig_i^{r,I} + \frac{V_i^{r,I}}{Kg_i^I} \right) - \frac{V_{k_i}^2}{Kg_i^I} \right] \quad (17)$$

$$Pg_{tot}^R = \sum_{i \in \mathcal{G}^R} Pg_i^R \quad (18)$$

$$Pd_{tot} = \sum_{i \in \mathcal{D}} Pd_i \quad (19)$$

$$P_{tot}^{loss} = \sum_{j=1}^{N^{bran}} P_j^{loss} = \sum_{j=1}^{N^{bran}} g_j^{bran} (V_{k_j} - V_{m_j})^2 \quad (20)$$

\mathcal{G}^P , \mathcal{G}^I and \mathcal{G}^R are the DG sets associated with power-based droop control, current based droop control and renewable energy resources.

$$\mathcal{G} = (\mathcal{G}^P \cup \mathcal{G}^I \cup \mathcal{G}^R)$$

Pg_{tot}^P and Pg_{tot}^I are the total power generation for the DG with droop control based on power and current, respectively.

Pg_{tot}^R is the total power generation for renewable DG.

Pg_i^R is the power output for renewable DG i .

Pd_{tot} is the total power associated with the microgrid loads.

$P_j^{loss} = g_j^{bran} (V_{k_j} - V_{m_j})^2$ is the resistive loss in branch j .

g_j^{bran} is the series conductance for branch j .

P_{tot}^{loss} is the total power related to resistive losses in the branches.

At this point, it is interesting to mention that the equivalent circuit of the network used to evaluate the voltage components related to the voltage sources has no connection with the ground, since generators and

loads are modeled as current sources that are replaced by open circuits due to the principle of superposition. Therefore, the voltage components related to voltage sources are all equal to V_1 . Consequently, the nodal voltage in an iteration of the FMF-DC is defined as follows:

$$V_k^{(\tau)} = V_k^{CS^{(\tau)}} + V_1^{(\tau)} \quad \forall k = 1, \dots, N^{node} \quad (21)$$

Where:

$V_k^{(\tau)}$ is the voltage in the node k for the iteration τ .

$V_k^{CS^{(\tau)}}$ is the voltage component related to the current source at node k for iteration τ . This component is determined using a backward/forward sweep for radial DC microgrids and MANA for meshed DC microgrids. In both cases, the voltage source associated with the CCP is zero (short circuit) due to the superposition principle.

To obtain the power balance equation as a function of $V_1^{(\tau)}$, it is necessary to substitute (21) in each voltage dependent term in this equation. Therefore, the total losses and the total generation for DG with droop control are given by:

$$i) \underline{P_{tot}^{loss}^{(\tau)}}$$

$$P_{tot}^{loss^{(\tau)}} = \sum_{j=1}^{N^{bran}} g_j^{bran} (V_{k_j}^{(\tau)} - V_{m_j}^{(\tau)})^2 = \sum_{j=1}^{N^{bran}} g_j^{bran} (V_{k_j}^{CS^{(\tau)}} - V_{m_j}^{CS^{(\tau)}})^2 \quad (22)$$

Where $P_{tot}^{loss^{(\tau)}}$ are the total resistive losses for iteration τ . From (22), it can be concluded that the total resistive losses are functions only of the voltage components related to the current sources, since the voltage components related to the voltage sources ($V_1^{(\tau)}$) are cancelled by the voltage difference term, that is: $V_{k_j}^{(\tau)} - V_{m_j}^{(\tau)} = V_{k_j}^{CS^{(\tau)}} + V_1^{(\tau)} - (V_{m_j}^{CS^{(\tau)}} + V_1^{(\tau)}) = V_{k_j}^{CS^{(\tau)}} - V_{m_j}^{CS^{(\tau)}}$.

$$ii) \underline{P_{tot}^I} :$$

$$Pg_{tot}^I = a_{tot}^{g,I} \left[V_1^{(\tau)} \right]^2 + b_{tot}^{g,I} V_1^{(\tau)} + c_{tot}^{g,I} \quad (23)$$

Where:

$$a_{tot}^{g,I} = -\sum_{i \in \mathcal{G}^I} \left(\frac{1}{Kg_i^I} \right) \quad (24)$$

$$b_{tot}^{g,I} = \sum_{i \in \mathcal{G}^I} \left(Ig_i^{r,I} + \frac{V_i^{r,I} - 2V_{k_i}^{CS(\tau)}}{Kg_i^I} \right) \quad (25)$$

$$c_{tot}^{g,I} = \sum_{i \in \mathcal{G}^I} \left[\left(Ig_i^{r,I} + \frac{V_i^{r,I}}{Kg_i^I} \right) V_{k_i}^{CS} - \frac{\left(V_{k_i}^{CS(\tau)} \right)^2}{Kg_i^I} \right] \quad (26)$$

iii) Pg_{tot}^P :

$$Pg_{tot}^P = b_{tot}^{g,P} V_1^{(\tau)} + c_{tot}^{g,P} \quad (27)$$

Where:

$$b_{tot}^{g,P} = -\sum_{i \in \mathcal{G}^P} \left(\frac{1}{Kg_i^P} \right) \quad (28)$$

$$c_{tot}^{g,P} = \sum_{i \in \mathcal{G}^P} \left[Pg_i^{r,P} + \frac{V_i^{r,P}}{Kg_i^P} - \frac{V_{k_i}^{CS(\tau)}}{Kg_i^{PV}} \right] \quad (29)$$

The replacement of (22), (23) and (27) in the power balance equation (15) result in (30).

$$a_{tot}^{bal} \left[V_1^{(\tau)} \right]^2 + b_{tot}^{bal} V_1^{(\tau)} + c_{tot}^{bal} = 0 \quad (30)$$

Where:

$$a_{tot}^{bal} = a_{tot}^{g,I} \quad (31)$$

$$b_{tot}^{bal} = b_{tot}^{g,P} + b_{tot}^{g,I} \quad (32)$$

$$c_{tot}^{bal} = \left(c_{tot}^{g,P} + c_{tot}^{g,I} + P_{tot}^R - P_{tot}^{loss(\tau)} - P_{tot}^{load} \right) \quad (33)$$

From the equation (30), it can be concluded that the power balance equation is a quadratic function of $V_1^{(\tau)}$. Consequently, there are two solutions for $V_1^{(\tau)}$:

$$V_1^{(\tau)} = \left(-b_{tot}^{bal} + \sqrt{\left(b_{tot}^{bal} \right)^2 - 4a_{tot}^{bal} c_{tot}^{bal}} \right) / (2a_{tot}^{bal}) \quad (34)$$

$$V_1^{(\tau)} = \left(-b_{tot}^{bal} - \sqrt{\left(b_{tot}^{bal} \right)^2 - 4a_{tot}^{bal} c_{tot}^{bal}} \right) / (2a_{tot}^{bal}) \quad (35)$$

However, only the solution $V_1^{(\tau)}$ has physical meaning, since the solution $V_1^{(\tau)}$ can be associated with a negative voltage or a very low voltage. Once the voltage $V_1^{(\tau)}$ has been calculated, the remaining nodal voltages can be obtained using the superposition principle defined in (21). At this point, it is important to emphasize another important difference between FMS for AC and DC microgrids: the approach to solve the subproblem. In AC microgrids the solution of the subproblem requires an iterative procedure based on NRM. On the other hand, the solution of the subproblem in DC microgrids is simpler, since it is based on second degree polynomial roots.

Based on the theory described above, it is possible to evaluate the nodal voltages in radial DC microgrids using the algorithm presented in the flowchart of Fig. 4, where:

The input data for the FMS-DC for radial microgrids are: maximum

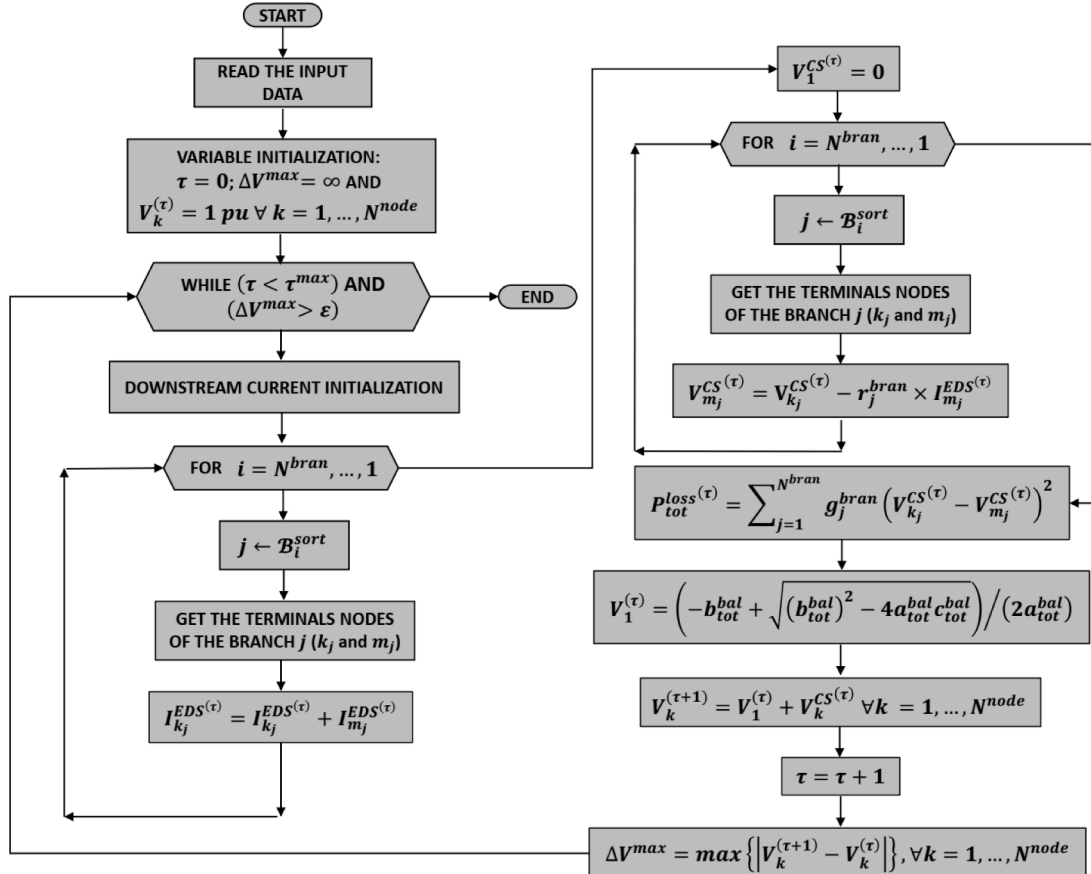


Fig. 4. Flowchart of the iterative FMS-DC algorithm for radial microgrids.

number of iterations τ^{max} , tolerance ε for the convergence test, \mathcal{S}^{sort} and data for branches, loads and DG.

ΔV^{max} is the maximum voltage deviation.

The block ‘‘Downstream Current Initialization’’ makes the following calculations:

$$I_k^{EDS^{(\tau)}} = 0 \quad \forall k = 1, \dots, N^{node} \quad (36)$$

$$I_{k_i}^{EDS^{(\tau)}} = I_{k_i}^{EDS^{(\tau)}} - I_{g_{k_i}}^{(\tau)}(V_{k_i}^{(\tau)}) \quad \forall i \in \mathcal{S} \quad (37)$$

$$I_k^{EDS^{(\tau)}} = I_k^{EDS^{(\tau)}} + Id_k^{(\tau)}(V_k^{(\tau)}) \quad \forall k \in \mathcal{S} \quad (38)$$

$I_{k_j}^{EDS^{(\tau)}}$ is the equivalent current downstream from the node k_j for the iteration (τ) .

$$Id_k^{(\tau)}(V_k^{(\tau)}) = \frac{Pd_k}{V_k^{(\tau)}} \quad \forall k \in \mathcal{S} \quad (39)$$

$$I_{g_{k_i}}^{(\tau)}(V_{k_i}^{(\tau)}) = \begin{cases} \frac{Pg_i^{r,P}}{V_{k_i}^{(\tau)}} + \frac{1}{Kg_i^P} \left(\frac{V_i^{r,P}}{V_{k_i}^{(\tau)}} - 1 \right), & i \in \mathcal{S}^P \\ Ig_i^{r,I} + \frac{1}{Kg_i^I} (V_i^{r,I} - V_{k_i}^{(\tau)}), & i \in \mathcal{S}^I \\ Pg_i^R / V_{k_i}^{(\tau)}, & i \in \mathcal{S}^R \end{cases} \quad (40)$$

The iterative procedure described in the flowchart of Fig. 4 can be expanded to meshed DC microgrids. In this case, the voltage components due to current sources are evaluated using GZM based on MANA instead of backward/forward sweep techniques. Consequently, the mathematical model of the linear electric circuit for meshed microgrids in an iteration of the GZM is defined according to (41) [19].

$$Ax = b \quad (41)$$

Where:

$$A = \begin{bmatrix} G & F^t \\ F & O \end{bmatrix} \quad (42)$$

$$b = \begin{bmatrix} I^{eq} \\ V^{spe} \end{bmatrix} \quad (43)$$

$$x = \begin{bmatrix} V \\ I^{vs} \end{bmatrix} \quad (44)$$

N^{volt} is the number of voltage sources. Normally, only the voltage associated with PCC is needed to evaluate the voltages in meshed microgrids. However, there may be additional voltage sources to model zero impedance branches, such as protection and normally closed switches.

A is the matrix of coefficients of the linear MANA system with dimension $(N^{node} + N^{volt}) \times (N^{node} + N^{volt})$.

G is the nodal conductance matrix of the microgrid with dimension $N^{node} \times N^{node}$.

F is the voltage source/node incidence matrix with dimension $N^{volt} \times N^{node}$. The elements of matrix F are as follows:

$$F_{ij} = \begin{cases} 1, & \text{if the } j\text{th node is the positive terminal for the } i\text{th voltage source} \\ -1, & \text{if the } j\text{th node is the negative terminal for the } i\text{th voltage source} \\ 0, & \text{if the } i\text{th voltage source is not incident to the } j\text{th node} \end{cases} \quad (45)$$

O is a $N^{volt} \times N^{volt}$ matrix of zeros.

V is a $N^{volt} \times 1$ vector associated with the microgrid voltages.

I^{vs} is a $N^{volt} \times 1$ vector that stores the unknown values of the voltage sources currents.

x is a $(N^{node} + N^{volt}) \times 1$ vector that is composed of the MANA state variables, that is, nodal voltages and voltage sources currents.

b is a $(N^{node} + N^{volt}) \times 1$ vector associated with the right side of the MANA system, that is, equivalent current injections and specified values for the voltage sources.

I^{eq} is a $N^{node} \times 1$ vector that contains current injections related to equivalent circuits for loads and DG.

V^{spe} is a $N^{volt} \times 1$ vector that contains the specified values for the voltage sources.

From the MANA formulation defined in (41), it is possible to evaluate the voltages in a meshed microgrid using the flowchart defined in Fig. 5, where the input data for the FMS-DC for meshed microgrids are: τ^{max} , ε , and data for branches, loads and DG.

5. Probabilistic Power Flow for DC Islanded Microgrids

Normally, the uncertainties of the microgrid are considered in planning studies through the PPF based on the MCS [7].

The MCS samples the uncertainties related to individual components to define a system state. In this paper, the state of the system is defined considering the uncertainties related to: load forecasting errors, variability of renewable DG and outages in DG and circuits. Consequently, the state of the system is defined according to (46).

$$\mathbb{X}^{S,[i]} = [\mathbb{X}^{D,[i]} \quad \mathbb{X}^{R,[i]} \quad \mathbb{X}^{G,[i]} \quad \mathbb{X}^{C,[i]}]^T \quad (46)$$

Where:

The superscript T denotes the transposition of a matrix or vector.

$\mathbb{X}^{S,[i]}$ is the i th system state with dimension $|\mathcal{S}| + |\mathcal{S}^R| + |\mathcal{S}| + N^{bran}$

$\mathbb{X}^{D,[i]}$ is the vector of sampled values of the active powers associated with the loads for the i th system state. The load forecasting error was modeled using the normal distribution [24],[25]. Consequently, the elements of the vector $\mathbb{X}^{D,[i]}$ are defined as follows [24],[25]:

$$\mathbb{X}_j^{D,[i]} = Pd_k + Z^{norm}(0, \sigma_k^{kw}) \quad \forall k \in \mathcal{S}; j = 1, \dots, |\mathcal{S}| \quad (47)$$

$$\sigma_k^{kw} = (\epsilon_{\%}^{kw} \times Pd_k) / 300 \quad (48)$$

$Z^{norm}(0, \sigma_k^{kw})$ is a Gaussian random variable with a mean of zero and a standard deviation σ_k^{kw} .

σ_k^{kw} is the standard deviation associated with the active power of the load at the node k .

$\epsilon_{\%}^{kw}$ is the load forecasting error in percentage.

$\mathbb{X}^{R,[i]}$ is the output power vector of the photovoltaic solar DG for the i th system state. The output power of the solar photovoltaic DG is a function of the solar irradiance which is a random variable. In this paper, solar irradiance was modelled using the beta distribution [26]. The $\mathbb{X}^{R,[i]}$ elements are defined according to (49)-(51) [26].

$$\mathbb{X}_j^{R,[i]} = Pg_i^R [Z^{beta}(\hat{\alpha}^{solar}, \hat{\beta}^{solar})] \quad \forall i \in \mathcal{S}^R; j = |\mathcal{S}| + 1, \dots, |\mathcal{S}| + |\mathcal{S}^R| \quad (49)$$

$$\hat{\beta}^{solar} = (1 - \hat{\mu}^{solar}) \times \left[\frac{\hat{\mu}^{solar} \times (1 + \hat{\mu}^{solar})}{\hat{\sigma}^{solar}} - 1 \right] \quad (50)$$

$$\hat{\alpha}^{solar} = \frac{\hat{\mu}^{solar} \times \hat{\beta}^{solar}}{(1 - \hat{\mu}^{solar})} \quad (51)$$

$Z^{beta}(\hat{\alpha}^{solar}, \hat{\beta}^{solar})$ is a random variable with beta distribution used to model solar radiation.

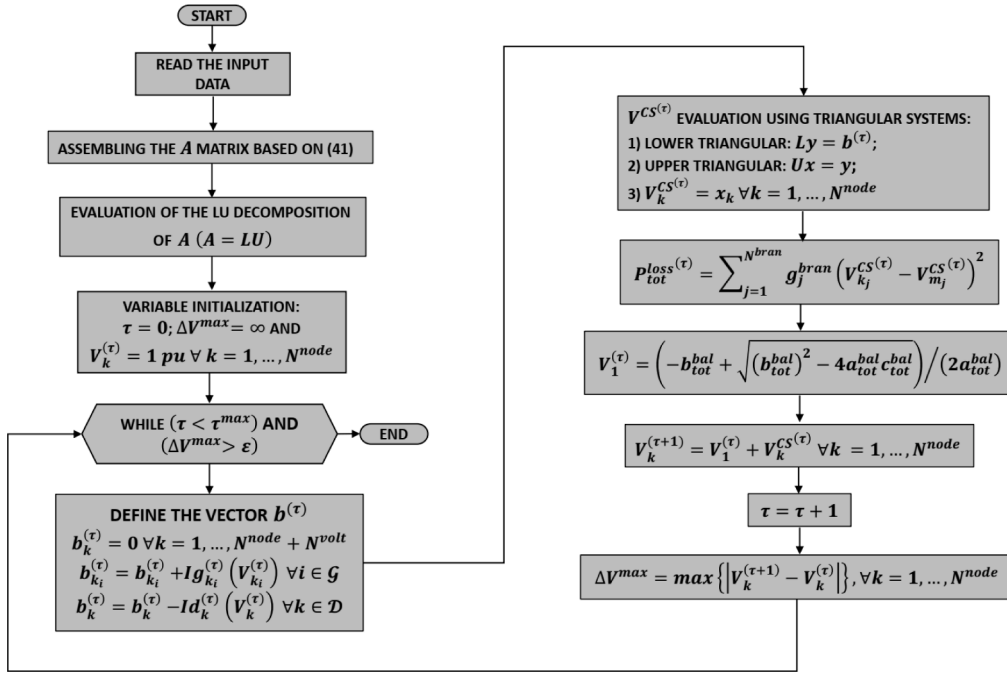


Fig. 5. Flowchart of the iterative FMS-DC algorithm for meshed microgrids.

$\hat{\alpha}^{solar}$ and $\hat{\beta}^{solar}$ are the parameters of the beta distribution used to model the solar radiation estimated by the method of moments.

$\hat{\mu}^{solar}$ and $\hat{\sigma}^{solar}$ are the mean and standard deviation estimated from the solar radiation data.

$Pg_i^R[Z^{beta}(\hat{\alpha}^{solar}, \hat{\beta}^{solar})]$ is the Pg_i^R as a function of the random variable $Z^{beta}(\hat{\alpha}^{solar}, \hat{\beta}^{solar})$. This function considers several typical parameters of PV solar DG, for example, short-circuit current, open-circuit voltage, nominal cell operating temperature, etc. A detailed description of the $Pg_i^R[Z^{beta}(\hat{\alpha}^{solar}, \hat{\beta}^{solar})]$ function is given in [26].

$\mathbb{X}^{G,[i]}$ and $\mathbb{X}^{C,[i]}$ are the vectors of component states associated with DG and circuits, respectively. In this paper it is considered that the availability of component is modeled using a two state Markovian [24]: operation and failure. In this way, the state vectors associated with the DG and circuit unavailability are sampled as follows:

$$\mathbb{X}_j^{G,[i]} = \begin{cases} 0 \text{ (operation)}, & \text{if } 0 \leq X^{uni} \leq U_k^G \forall k = 1, \dots, |\mathcal{G}|; j \\ 1 \text{ (repair)}, & \text{if } U_k^G \leq X^{uni} < 1.0 \end{cases} \quad \forall k = 1, \dots, |\mathcal{G}|; j$$

$$= |\mathcal{G}| + |\mathcal{R}| + k \quad (52)$$

$$\mathbb{X}_j^{C,[i]} = \begin{cases} 0 \text{ (operation)}, & \text{if } 0 \leq X^{uni} \leq U_m^C \forall m = 1, \dots, N^{bran}; j \\ 1 \text{ (repair)}, & \text{if } U_m^C \leq X^{uni} < 1.0 \end{cases}$$

$$= |\mathcal{G}| + |\mathcal{R}| + |\mathcal{C}| + m \quad (53)$$

U_k^G and U_m^C are the failure probabilities for DG k and circuit m , respectively.

In this paper, it was considered that a circuit failure results in the outage of only the component in which the fault occurred. In other words, the fault is eliminated by the protection devices at the terminals of the branches. This assumption is consistent with the operation of medium and low voltage meshed microgrids, since each branch of these microgrids is equipped with bidirectional current relays and fault limiters, respectively. In addition, after the failed component is isolated by its protection devices, it is necessary to perform topological processing to identify and eliminate the components isolated from the power sources.

After a system state is sampled, FMS-DC (iterative or approximated)

is performed to determine the microgrid voltages. These voltages are used to estimate performance indices, such as total resistive losses. The system state draw is repeated to generate a sample with the specified sample size. From this sample, it is possible to estimate probabilistic indices using the definition of average value as follows:

$$\bar{E}[F] = \frac{1}{N^{samp}} \sum_{i=1}^{N^{samp}} F[\mathbb{X}^{S,[i]}] \quad (54)$$

Where: N^{samp} is the specified sample size and $F[\mathbb{X}^{S,[i]}]$ is the test-function for the i th system state associated with an index of interest. For example, the test function for risk of voltage violation at a given node is defined as follows:

$$F[\mathbb{X}^{S,[i]}] = \begin{cases} 1, & V_k^{min} > V_k^{[i]} > V_k^{max} \\ 0, & \text{otherwise} \end{cases} \quad (55)$$

Where: $V_k^{[i]}$ is the voltage at node k for the i th system state and V_k^{min} (V_k^{max}) is the minimum (maximum) voltage limit for node k . Therefore, voltage violation risk expresses the probability of a nodal voltage going outside the upper and lower bounds established by the grid code.

6. Tests Results

6.1. Characteristics of Test-Systems and Definition of Case Studies

The FMS-DC algorithms proposed in this paper were tested in DC microgrids obtained from modifications in existing AC microgrids. The modifications made consist of disregarding the reactance of the branches and the reactive power of the loads [27]. The following DC microgrids were used in this paper:

- i) 33-node microgrid with radial and meshed topologies (MG-33): based on the radial microgrid proposed in [20]. The voltage level for the MG-33 with radial and meshed topologies is 12.66 kV DC.
- ii) 906-node radial microgrid (MG-906): this microgrid is based on the low voltage radial European distribution network with 906 nodes proposed in [21]. The voltage level on the MG-906 is 3kV

DC. The European distribution network is unbalanced. As a result, the following assumptions were considered in the generation of the MG-906: (i) branches resistances were obtained from positive sequence resistances; (ii) the loads of the individual phases were added to achieve the equivalent three-phase load. In addition, 2,000 kW DG were allocated to the MG-906 according to the GIS diagram in Fig. 6.

iii) 144-node meshed microgrid (MG-144): based on the American low voltage meshed network proposed in [21]. In this microgrid, 20 DG DC of 1600 kW were allocated to the following nodes: S1, S6, S11, S16, S21, S42, S47, S52, S57, S62, S83, S88, S93, S98, S103, S124, S129, S134, S139 and S144. The voltage level considered in the MG-144 is 380V DC.

The iterative and approximate FMS-DC introduced in this paper were validated considering the following case studies:

- i) **Deterministic:** evaluation of the voltage in the MG-33 with radial and meshed topologies. In this case, the DG located at nodes 1 and 33 have current based droop control and the DG installed nodes 6, 13, and 25 has power-based droop control.
- ii) **Probabilistic:** estimation of probabilistic indices using PPF based on MCS in MG-906 and MG-144. In this case study, it was considered that half of the DGs are solar renewable and the remaining DGs are conventional fossils. In addition, it was assumed that half of the DG has power-based droop control and the remaining DG has current-based droop control. In the MG-906, the uncertainties in the following parameters of the microgrid were considered: load, output of renewable DG and unavailability of DG. On the other hand, in the MG-144, the uncertainties in the unavailability of the circuits were considered in addition to those included in the MG-906. The PPF study was carried out considering that the Forced Outage Rate (FOR) is equal to 4% for renewable and conventional DG. The data necessary to include load forecasting errors, branch outages and variability of solar irradiation in the probabilistic power flow can be obtained in [28] and [29].

The NRM was used in two case studies specified above to provide a reference to assess the accuracy and computational cost of the proposed FMS-DC algorithms. The algorithms compared to the NRM are designated as follows:

- i) **FMS-ASM1:** approximate FMS-DC based on ASM with linear circuits for loads and DG obtained through the Taylor expansion series.

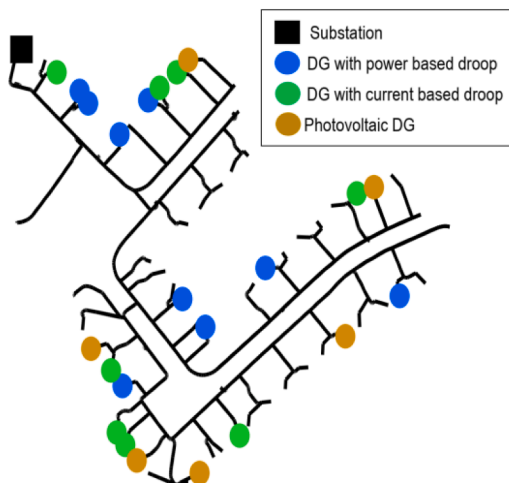


Fig. 6. GIS diagram of MG-906 showing DG allocation (circles).

- ii) **FMS-ASM2:** approximate FMS-DC based on ASM with linear circuits for loads and DG obtained by linear regression.
- iii) **FMS-CSM:** iterative FMS-DC based on CSM.
- iv) **FMS-GZM:** iterative FMS-DC based on GZM with MANA.

Finally, it is important to identify the following application scenarios for the iterative and approximate algorithms in the scope of test-systems:

- i) **Approximate:** FMS-ASM1 and FMS-ASM2 can only be applied in radial microgrids, as they are based on the backward/forward sweep technique. Thus, the deterministic and probabilistic tests with these methods were performed on the MG-33 with radial topology and on the MG-906, respectively.
- ii) **Iterative:** FMS-CSM can only solve FMS-DC in radial microgrids as it is based on backward/forward sweep technique. Consequently, deterministic and probabilistic tests with this method were also performed on the MG-33 version with radial topology and MG-906, respectively. On the other hand, FMS-GZM can solve FMS-DC in radial and meshed microgrids, as it is based on GZM with MANA. Thus, the deterministic and probabilistic tests with this method were performed on the MG-33 with meshed topology and MG-144, respectively.

The applications scenarios specified above are summarized in Table 1, where the cell elements “Det.,” “Prob.” and “X” are associated with deterministic tests, probabilistic tests and without application scenario, respectively.

6.2. Deterministic Case

Fig. 7 shows the voltage profiles on the MG-33 with radial and meshed topology. In addition, Table 2 presents some statistics associated with the relative error (in relation to the NRM) for nodal voltages in this microgrid. From Fig. 7 and Table 2, it can be concluded that the voltages calculated by the proposed FMS-DC present good accuracy in relation to the NRM.

Table 3 presents the output powers of the DG and the total losses in the MG-33 with radial and meshed topology obtained by the proposed methods and NRM. In addition, this table shows the relative errors for these variables in relation to the NRM. From this table, it can be noted that the proposed methods also provide very accurate estimates for the losses and output powers of the DG. From the Tables 2 and 3, it can be concluded that: the accuracy of the approximate FMS-DC algorithms based on the linear regression is better than those based on the Taylor expansion.

6.3. Probabilistic Case

This subsection presents the results obtained by the PPF based on the proposed FMS-DC. These results were obtained considering that $N^{samp} = 50000$. Fig. 8 shows the risk of voltage violation for the nodes of MG-906 and MG-144.

Additionally, Fig. 9 presents the probability density functions of the total losses in these microgrids. From these figures, it can be concluded that the PPF based on the proposed FMS-DC produces probabilistic

Table 1
Specification of the application scenario for the approximate and iterative FMS-DC algorithms

Microgrid	Topology	Approximate		Iterative	
		FMS-ASM1	FMS-ASM2	FMS-CSM	FMS-GZM
MG-33	Radial	Det.	Det.	Det.	X
MG-33	Meshed	X	X	X	Det.
MG-144	Meshed	X	X	X	Prob.
MG-906	Radial	Prob.	Prob.	Prob.	X

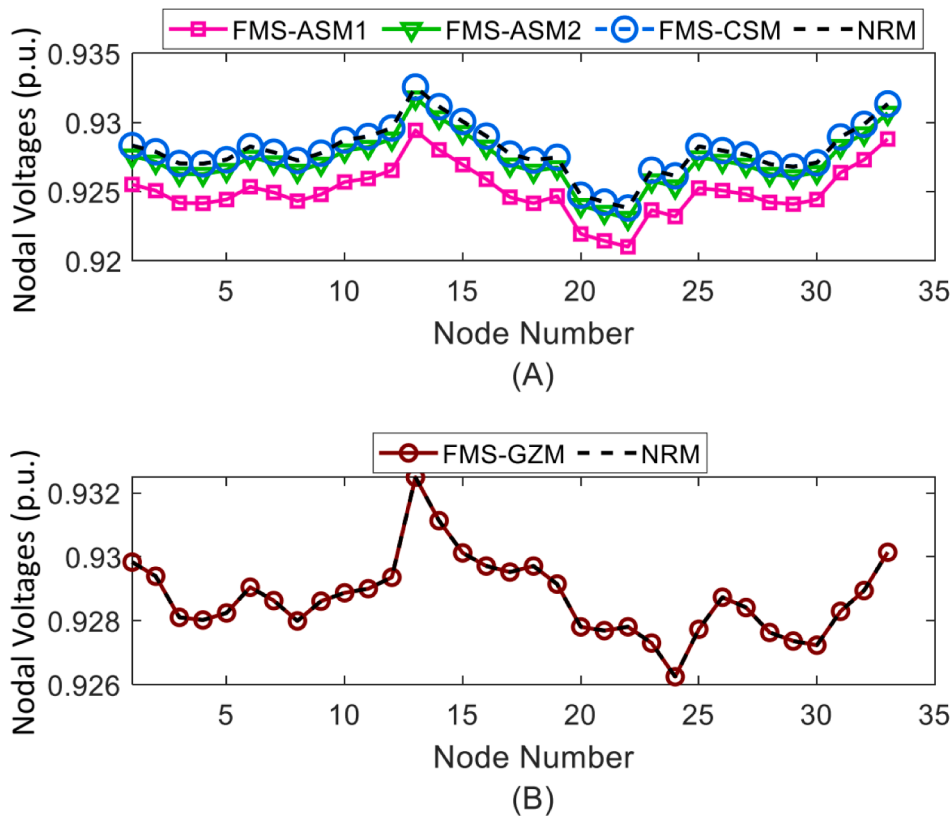


Fig. 7. Voltage profile in MG-33: (A) Radial (B) Meshed.

Table 2
Nodal voltage relative error Statistics (in percentage) on the MG-33.

Statistics	Radial FMS- ASM1	FMS- ASM2	FMS-CSM	Meshed FMS-GZM
Mean	0.311673	0.080544	2.0358×10^{-6}	1.1661×10^{-6}
Standard Deviation	0.017907	0.003777	1.6176×10^{-6}	5.2788×10^{-7}
Minimum	0.272278	0.070862	6.8745×10^{-8}	4.5490×10^{-8}
Maximum	0.336159	0.086218	4.9525×10^{-6}	2.5074×10^{-6}

indices that are very close to those generated by the PPF based on the NRM. Table 4 presents some statistics related to the total losses in MG-906 and MG-144. In addition, this table shows the relative absolute

Table 3
DG output powers, losses, and relative errors (in parentheses) in the MG-33.

Index	Radial FMS-ASM1	FMS-ASM2	FMS-CSM	NRM	Meshed FMS-GZM	NRM
$P_{G6}^p(V_6)$ (p.u.)	1.57177 (1.69046%)	1.55247 (0.44162%)	1.545641 (0%)	1.545641 (0%)	1.538545 (0%)	1.538545 (0%)
$P_{G13}^p(V_{13})$ (p.u.)	1.53506 (1.86887%)	1.51394 (0.46744%)	1.506893 (0%)	1.506893 (0%)	1.507581 (0%)	1.507581 (0%)
$P_{G25}^p(V_{25})$ (p.u.)	1.57261 (1.75095%)	1.55275 (0.46605%)	1.545550 (0%)	1.545550 (0%)	1.550392 (0%)	1.550392 (0%)
$P_{G1}^l(V_1)$ (p.u.)	1.45333 (1.32759%)	1.43929 (0.34913%)	1.434287 (0%)	1.434287 (0%)	1.424025 (0%)	1.424025 (0%)
$P_{G33}^p(V_{33})$ (p.u.)	1.43103 (1.22720%)	1.41821 (0.32018%)	1.413683 (0%)	1.412972 (0%)	1.421924 (0%)	1.421924 (0%)
P_{tot}^{loss} (p.u.)	0.016038 (0.10051%)	0.016057 (0.01916%)	0.016054 (0%)	0.016054 (0%)	0.012467 (0%)	0.012467 (0%)

errors (in percentage) associated with the indices estimated by FMS-ASM1 and FMS-ASM2. These relative errors were calculated considering the NRM indices as reference values. For example, relative absolute errors for FMS-ASM1 are given by:

$$Err_{ASM1}^{Stat} = 100\% \left| \frac{Stat_{ASM1} - Stat_{NRM}}{Stat_{NRM}} \right| \quad (56)$$

Where:

$Stat_{ASM1}$ and $Stat_{NRM}$ are the statistics estimated by PPF based on FMS-ASM1 and NRM, respectively.

Err_{ASM1}^{Stat} is the relative absolute error in percentage associated with the statistics $Stat$ estimated by PPF based on FMS-ASM1.

The relative absolute errors associated with FMS-ASM1 and FMS-ASM2 are identified by the numbers in parentheses below the indices in the second and third columns of Table 4, respectively. Based on the

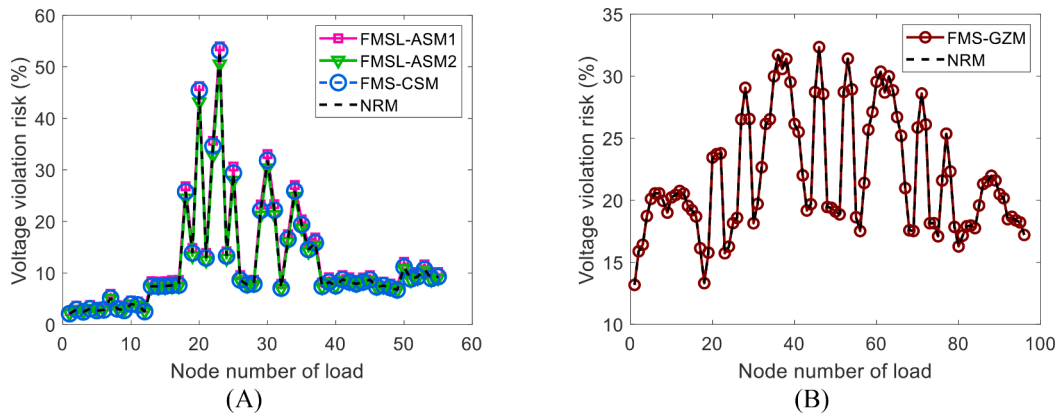


Fig. 8. Voltage violation risks: (A) MG-906 (B) MG-144.

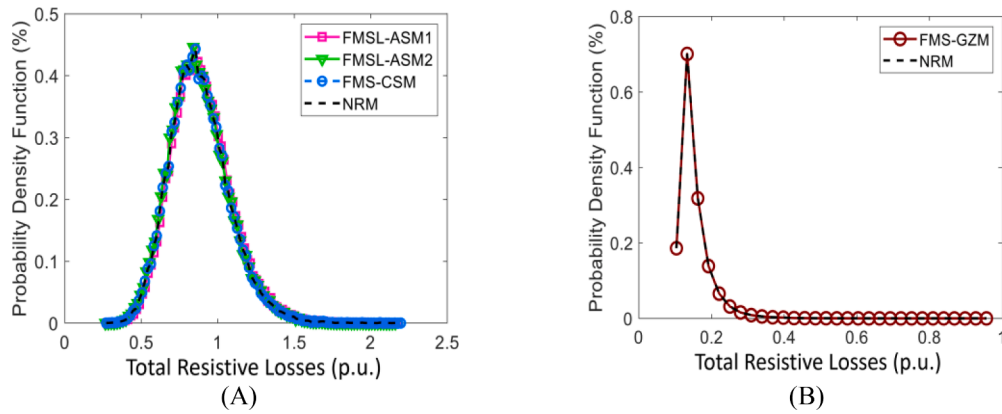


Fig. 9. Losses Probability distributions: (A) MG-906 (B) MG-144.

Table 4

Total Losses statistics for the MG-906 and MG-144 (CI-Confidence Interval for significance level of 95%).

Statistics to p_{tot}^{loss} (p.u.)	MG-906		FMS-CSM	NRM	MG-144	
	FMS-ASM1	FMS-ASM2			FMS-GZM	NRM
Lower Quartile	0.7497 (0.6714%)	0.7449 (0.0269%)	0.7447	0.7447	0.1243	0.1243
Median	0.8698 (0.7179%)	0.8648 (0.1390%)	0.8636	0.8636	0.1388	0.1388
Upper Quartile	1.0053 (0.7315%)	1.0004 (0.2405%)	0.9980	0.9980	0.1652	0.1652
Mean	0.8865 (0.6929%)	0.8817 (0.1477%)	0.8804	0.8804	0.1518	0.1518
Std. Deviation	0.1976 (0.4575%)	0.1979 (0.6101%)	0.1967	0.1967	0.0435	0.0435
CI Lower Bound	0.5427 (0.7051%)	0.5383 (0.1113%)	0.5389	0.5389	0.1092	0.1092
CI Upper Bound	1.3217 (0.5477%)	1.3182 (0.2815%)	1.3145	1.3145	0.2664	0.2664

relative absolute errors, it can be concluded that the FMS-ASM1 and the FMS-ASM2 have high accuracy for practical applications in relation to the NRM, despite the approximations considered in the derivation of these methods. For example, the maximum relative error for the

statistical indices calculated using FMS-ASM1 and FMS-ASM2 are equal to 0.7315% and 0.6101%, respectively. Additionally, Table 4 also showed that the statistical indices estimated through the proposed PPF based on the FMS-CSM and FMS-GZM exactly coincide with those

Table 5

Computational costs of the PPF based on NRM and proposed FMS-DC

Index	MG-906		FMS-CSM	NRM	MG-144	
	FMS-ASM1	FMS-ASM2			FMS-GZM	NRM
Time (sec.)	22.105672	22.663284	102.323321	3292.190891	80.000041	122.159340
Gain	148.9297	145.2654	32.1744	1	1.5270	1

obtained through the PPF based on the NRM.

Finally, Table 5 presents the CPU times and gains (in relation to the NRM) associated with the PPF based on the proposed FMS-DC and NRM. From this table, it can be concluded that the proposed FMS obtained a very significant saving in the PPF CPU time. It is interesting to note that the biggest gains are associated with the approximate backward/forward sweep methods, since these methods are free of linear systems solution and iterative processes. For example, the maximum gain (about 149) was achieved by the FMS-ASM1.

7. Conclusions

This paper presented approximate and iterative power flow algorithms for islanded Direct Current microgrids with radial and meshed topologies. These algorithms were developed based on the combination of the following techniques: Admittance Summation Method, Current Summation Method, Gauss-Zbus Method, Modified Augmented Nodal Analysis and Superposition Principle. The proposed algorithms were embedded in a Probabilistic Power Flow, based on Monte Carlo Simulation, in order to demonstrate that these algorithms are suitable for planning studies under uncertainties. The tests results with large scale microgrids demonstrate that the proposed algorithms have good accuracy in relation to the Newton-Raphson Method in the evaluation of the voltage profile and losses. In addition, the proposed methods achieve significant reductions in the computational cost associated with the Probabilistic Power Flow. Future work associated with the proposed power flow algorithms is oriented to towards expanding these algorithms to model the following aspects related to DC microgrids: secondary control, voltage unbalance in bipolar configuration and networked (interconnected) microgrids.

CRedit authorship contribution statement

Elson N.M. Silva: Conceptualization, Methodology, Software, Writing – original draft. **Anselmo B. Rodrigues:** Conceptualization, Methodology, Writing – review & editing. **Maria da Guia da Silva:** Conceptualization, Methodology, Writing – review & editing.

Declaration of Competing Interest

No Data

References

- [1] N. Hatziargyriou, *Microgrids: Architectures and Control*, 1st ed., Wiley-IEEE Press, Chichester, UK, 2014.
- [2] D.E. Olivares, A. Mehrizi-Sani, A.H. Etemadi, et al., Trends in Microgrid Control, *IEEE Trans. on Smart Grid* 5 (4) (July, 2014) 1905–1919.
- [3] A.T. Elsayed, A.A. Mohamed, O.A. Mohammed, DC microgrids and distribution systems: An overview, *Electric Power Systems Research* 119 (Feb. 2015) 407–417.
- [4] T. Dragičević T, P. Wheeler, F. Blaabjerg, *DC Distribution Systems and Microgrids*, 1st ed., UK, IET, Stevenage, 2018.
- [5] J.J. Justo, F. Mwasilu, J. Lee, J.W. Jung, AC-microgrids versus DC-microgrids with distributed energy resources: A review, *Renewable and Sustainable Energy Reviews* 24 (Aug. 2013) 387–405.
- [6] P. Wang, L. Goel, X. Liu, F.H. Choo, Harmonizing AC and DC: A Hybrid AC/DC Future Grid Solution, *IEEE Power and Energy Magazine* 11 (3) (May-June 2013) 76–83.
- [7] B.R. Prusty, D. Jena, A critical review on probabilistic load flow studies in uncertainty constrained power systems with photovoltaic generation and a new approach, *Renewable and Sustainable Energy Reviews* 69 (Mar. 2017) 1286–1302.
- [8] S. Fan, X. Liu, Y. Yang, et al., “Power flow calculation method for DC distribution system with voltage source converter operation mode consideration,” *IOP Conference Series: Earth and Environmental Science*, vol. 227, no. 3, e032046, doi: <https://doi.org/10.1088/1755-1315/227/3/032046>.
- [9] A. Garces, On the Convergence of Newton’s Method in Power Flow Studies for DC Microgrids, *IEEE Trans. on Power Systems* 33 (5) (Sept. 2018) 5770–5777.
- [10] C. Li, S.K. Chaudhary, M. Savaghebi, J.C. Vasquez, J.M. Guerrero, Power Flow Analysis for Low-Voltage AC and DC Microgrids Considering Droop Control and Virtual Impedance, *IEEE Trans. on Smart Grid* 8 (6) (Nov. 2017) 2754–2764.
- [11] R. Asad, A.A. Kazemi, Novel slack bus-free load flow method for dc microgrids and distribution systems with dc-bus signaling control methods, *International Transactions on Electrical Energy Systems* 25 (12) (Dec. 2015) 3538–3552.
- [12] A. Garces, Uniqueness of the power flow solutions in low voltage direct current grids, *Electric Power Systems Research* 151 (Oct. 2017) 149–153.
- [13] A. Maulik, D. Das, Application of linearized load flow method for droop controlled DCMGs, *IET Generation, Transmission & Distribution* 14 (6) (Mar. 2020) 1114–1126.
- [14] O.D. Montoya, L.F. Grisales-Noreña, D. González-Montoya, C. Ramos-Paja, A. Garces, Linear power flow formulation for low voltage DC power grids, *Electric Power Systems Research* 163 (Oct. 2018) 375–381.
- [15] D. Rajcic, R. Taleski, Two novel methods for radial and weakly meshed network analysis, *Electric Power Systems Research* 48 (2) (Dec. 1998) 79–87.
- [16] D. Shirmohammadi, H.W. Hong, A. Semlyen, G.X. Luo, A compensation-based power flow method for weakly meshed distribution and transmission networks, *IEEE Trans. Power Systems* 3 (2) (May 1998) 753–762.
- [17] I. Kocar, J. Mahseredjian, U. Karaagac, G. Soykan, O. Saad, Multiphase Load-Flow Solution for Large-Scale Distribution Systems Using MANA, *IEEE Trans. Power Delivery* 29 (2) (Apr. 2014) 908–915.
- [18] T.H. Chen, M.S. Chen, K.J. Hwang, P. Kotas, E.A. Chebli, Distribution system power flow analysis—a rigid approach, *IEEE Trans. Power Delivery* 6 (3) (July 1991) 1146–1152.
- [19] E.N.M. Silva, A.B. Rodrigues, M.G. Silva, Multi-slack power flow for islanded microgrids with radial and meshed topologies, *IET Generation, Transmission & Distribution* 14 (13) (July 2020) 2498–2509.
- [20] F. Hameed, M.A. Hosani, H.H. Zeineldin, A Modified Backward/Forward Sweep Load Flow Method for Islanded Radial Microgrids, *IEEE Trans. Smart Grid* 10 (1) (Jan. 2019) 910–918.
- [21] IEEE PES Distribution Systems Analysis Subcommittee Radial Test Feeders. [Online]. Available: <http://www.ewh.ieee.org/soc/pes/dsacom/testfeeders/index.html>. Accessed: May 2017.
- [22] A. Garces, A Linear Three-Phase Load Flow for Power Distribution Systems, *IEEE Trans. on Power Systems* 31 (1) (Jan. 2016) 827–828.
- [23] H. Ahmadi, J.R. Martí, A.A. von Meier, Linear Power Flow Formulation for Three-Phase Distribution Systems, *IEEE Trans. on Power Systems* 31 (6) (Nov. 2016) 5012–5021.
- [24] R. Billinton, W. Li, *Reliability Assessment of Electric Power Systems Using Monte Carlo Methods*, 1st ed., Springer, New York: USA, 1994.
- [25] R. Singh, B.C. Pal, R.B. Vinter, Measurement Placement in Distribution System State Estimation, *IEEE Trans. on Power Systems* 24 (2) (May 2009) 668–675.
- [26] Y.M. Atwa, E.F. El-Saadany, M.M.A. Salama MMA, R. Seethapathy, Optimal Renewable Resources Mix for Distribution System Energy Loss Minimization, *IEEE Trans. on Power Systems* 25 (1) (Feb. 2010) 360–370.
- [27] O.D. Montoya, W. Gil-González, A. Garces, Numerical methods for power flow analysis in DC networks: State of the art, methods and challenges, *International Journal of Electrical Power and Energy Systems* 123 (Dec. 2020), e106299, <https://doi.org/10.1016/j.ijepes.2020.106299>.
- [28] E.N.M. Silva, E. Chagas, A.B. Rodrigues, M.G. Silva, Linear Probabilistic Power Flow for Islanded Microgrids, in: 2020 International Conference on Probabilistic Methods Applied to Power Systems (PMAPS 2020), Liege, Belgium, 2020, <https://doi.org/10.1109/PMAPS47429.2020.9183485>.
- [29] M. Sengupta, Y. Xie, A. Lopez, A. Habte, G. Maclaurin, J. Shelby, The national solar radiation data base (NSRDB), *Renewable and Sustainable Energy Reviews* 89 (June 2018) 51–60.